Highlights

Modeling of the response function of CdTe detectors for a hard X-ray synthetic diagnostic

D. Choi, S. Coda, J. Decker, Y. Peysson, and the TCV team[1]

- A realistic response function is modeled for the CdTe detectors used in a hard X-ray diagnostic of the TCV tokamak
- The characteristics of the detector observed in the measurement of multiple radioactive sources are considered in the modeling
- The measured energy spectra of radioactive sources can be correctly reconstructed using the new response function
- The response function is applied to a hard X-ray synthetic diagnostic for the study of energetic electrons

[1]See author list of S. Coda et al 2019 Nucl. Fusion **59** 112023

Modeling of the response function of CdTe detectors for a hard X-ray synthetic diagnostic

D. Choi[a], S. Coda[a], J. Decker[a], Y. Peysson[b], and the TCV team[1a]

[a]*Ecole Polytechnique Fédérale de Lausanne (EPFL), Swiss Plasma Center (SPC), CH-1015 Lausanne, Switzerland*
[b]*CEA, IRFM, F-13108, Saint-Paul-lez-Durance, France*

Abstract

The response function of CdTe detectors used in a hard X-ray spectrometer system (HXRS) on the TCV tokamak fusion experiment is modeled based on the measured energy spectra from multiple gamma-ray sources. The response function consists of an asymmetric Gaussian photopeak, an exponentially inclined shelf structure below the photopeak, and CdTe escape peaks. It is demonstrated that the measured energy spectra of radioactive sources can be correctly reconstructed using this response function. This model is applied to a hard X-ray synthetic diagnostic used to convert a modeled electron distribution function to a measured hard X-ray signal, for the study of energetic electrons in the TCV tokamak.

Keywords:
Hard X-ray detection, Detector response function, CdTe sensor, Hard X-ray synthetic diagnostic

1. Introduction

Hard X-ray spectrometry is a key measurement technique for the study of highly energetic electrons in a tokamak plasma of thermonuclear interest [1]. To compare the measured bremsstrahlung radiation emitted by the high-energy tail of the electron distribution function with theoretical predictions, a so-called "synthetic diagnostic" is used. The synthetic diagnostic estimate, which can be directly compared to the measured count rate, is calculated

[1]See author list of S. Coda et al 2019 Nucl. Fusion **59** 112023

from Fokker-Planck modeling of the electron distribution function, using the bremsstrahlung cross section and the detector's efficiency and response function [2].

In the Fokker-Planck modeling study of the energetic electrons, one of the primary goals is to understand their anomalous transport behavior during various plasma operation scenarios. For this purpose the energetic electron transport term in the Fokker-Planck equation has been used as a free parameter in the simulation[3, 4, 5, 6, 7]. Therefore the other input parameters, such as plasma profiles or the machine specifications, are required to be accurate for a reliable simulation. In the hard X-ray synthetic diagnostic, the geometry and the response function of detectors have to be provided correctly to estimate the hard X-ray measurement.

The TCV tokamak [8] is characterized by high Electron Cyclotron Heating power and a significant resulting energetic-electron population, whose energy ranges from 10 keV to 300 keV, whereas the thermal electron temperature is near 2 keV. This tokamak features a hard X-ray tomographic spectrometer system (HXRS), which consists of four cameras comprising 101 CdTe detectors, whose lines of sight cover the entire poloidal plane, enabling a tomographic reconstruction. The detection of photons in the energy range between 10 keV and 300 keV is followed by electronic pulse processing and digital pulse processing chains [9, 10, 11].

The three-dimensional relativistic bounce-averaged Fokker-Planck code LUKE [12] and the fast electron bremsstrahlung code R5-X2 [2] are capable of calculating HXRS synthetic diagnostic estimates for TCV plasmas. However, the response function currently used in the synthetic diagnostic package R5-X2 [2, 13], which includes only the photopeak and the Compton continuum, deviates from the real response of the CdTe detector. The apparent energy spectrum produced by gamma-ray sources observed during detector calibration consists of a photopeak and a long shelf structure below the photopeak, due to both the Compton continuum and incomplete charge collection, which is a well-known feature of semiconductor detectors [14, 15, 16, 17]. Since the response function depends on each detector's specific characteristics such as structure, geometry, and composition, it appears necessary to put forward a model for the response function.

In this work, we present a response function model for the CdTe detectors employed in the HXRS apparatus in the TCV tokamak, based on the measurement of the energy spectra from five radioactive sources. Section 2 overviews the measurement setup and the spectroscopic features of the mea-

sured energy spectra. Section 3 describes the response function model and its coefficients, which are empirically determined from the measurement. Section 4 demonstrates the ability of the modeled response function to correctly reproduce the measured energy spectra, which is superior to the one which is currently implemented in the synthetic diagnostic module. Section 5 provides an example of an application of the modeled response function in the Fokker-Planck modeling procedure, where a comparison between simulation and measurement was made. A summary can be found in section 6.

2. Measurement of radioactive sources

2.1. Measurement setup

In order to analyze the response of the detector to monochromatic photons with varying energy, five energy spectra are measured using four radioactive isotopes, ^{241}Am, ^{109}Cd, ^{139}Ce, and ^{152}Eu, and a multi-isotope source, which is a liquid mixture of ^{133}Ba, ^{60}Co, and ^{137}Cs. The main gamma-ray and fluorescent X-ray energies of the sources are listed in Table 1 with their activities at the measurement date [18].

Radioactive source	Activity (kBq)	Gamma-rays (keV)	X-rays (keV)
Cerium-139	33.3	165.9	33.4, 33.0
Cadmium-109	12.7	88.0	22.2, 22.0
Europium-152	22.3	121.8, 244.7, 344.3, 778.9	40.1, 39.5
Americium-241	35.8	59.5	-
Multi-isotope source			
Barium-133	45.6	81.0, 276.4, 302.9, 356.0	31.0, 30.6
Cobalt-60	39.5	1332.5, 1173.2	-
Caesium-137	67.7	661.7	-

Table 1: Main gamma-ray and fluorescent X-ray energies of the radioactive sources.

During the measurement, each source is placed at 1 cm distance in front of a specific detector of one of the HXRS cameras. Both the camera and the radioactive source are shielded from natural background radiation by a lead cage. The detector is a 2 mm $\times$ 2 mm $\times$ 2 mm Ohmic-type CdTe (S.2.2.2U)

sensor, produced by Eurorad. The detector is connected to an in-house developed preamplifier card which is included in the camera set. The signal from the camera is processed through an Ortec 571 shaper/amplifier and then sent to Fast ComTec MCA-3, a PC-based, software controlled PCI-bus Multichannel Analyzer (MCA). 8129 channels are used and the threshold voltage is set to 0.4 V. Figure 1 shows a mapping from MCA channels to photon energies, by fitting the gamma-ray photopeaks of the measured spetra.

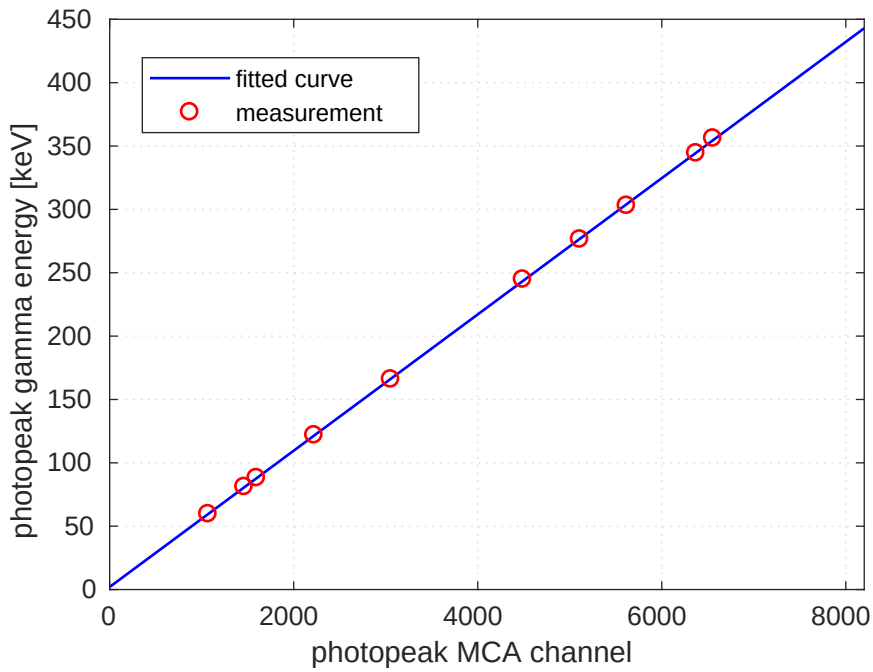

Figure 1: MCA channel - photon energy mapping.

2.2. Spectroscopic features

When a monochromatic photon beam with energy k impinges on the CdTe detector, the energy spectrum (counts per energy bin) is observed to have three distinct features: an asymmetric Gaussian photopeak near k, an exponentially inclined shelf structure below k, and escape peaks due to the CdTe material.

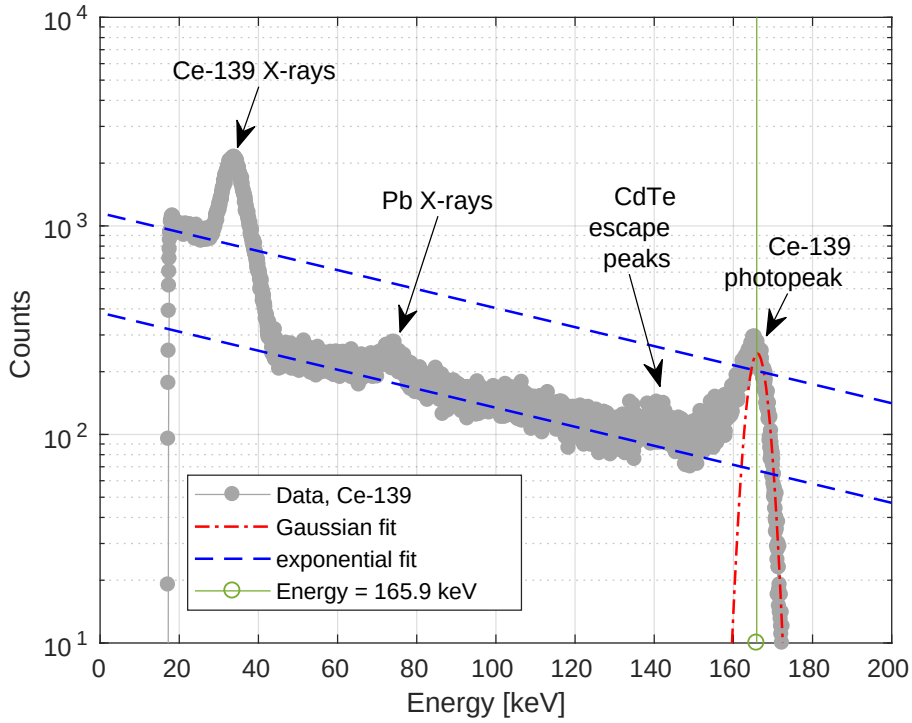

Figure 2: Measured energy spectrum from ^{139}Ce.

As an example, these characteristics can be seen in Figure 2, the measured energy spectrum from ^{139}Ce. Firstly, the photopeak deviates from a Gaussian fit at energies less than the gamma-ray energy, 165.9 keV, due to hole tailing that arises from charge trapping events, while the Gaussian curve fits the spectrum well for energies above 165.9 keV. This hole tailing can occur when charges created within the detector volume, such as holes and electrons, cannot reach the electrode by the crystal defects in the semiconductor. Then the lower number of collected charges gives lower pulse peak and in turn creates tail-like spectrum.

Below the photopeak, an inclined shelf, which can be attributed to a combination of the Compton continuum, incomplete charge collection and the interactions between the metal contact and the detector [11], is observed. This inclined shelf structure can be fitted by an exponential (blue dashed line in FIgure 2). The CdTe escape peaks are theoretically expected to appear at 142.7 keV and 139.8 keV, which correspond to the differences between the gamma-ray energy and the K_α line emission energies of Cd and Te, 23.2 keV and 26.1 keV. However, these peaks are observed to have a single broad peak due to their broad Gaussian shapes and the finite detector resolution.

In addition to the spectrum from the monochromatic gamma-ray, the fluorescent X-rays from ^{139}Ce also contribute to the total spectrum. Since the fluorescent X-ray peaks are closely spaced, a broad aggregate peak is observed around 30 keV. An additional inclined shelf structure is formed below the broad peak near 30 keV, as occurred below the photopeak of the gamma-ray at 165.9 keV. Lastly, there is a contribution from the fluorescent X-rays from the lead shielding near 75 keV, which also combine to form a single peak.

3. Modeling the response function

On the basis of the observed characteristics of the CdTe detector discussed in the previous section, the response function is modeled in this section, based on previous work on the modeling of semiconductor detector response [8-11]. In the case of a photon beam spectrum $\phi(k)$ impinging on the detector, the measured energy spectrum $M(E)$ can be expressed as

$$M(E) = \int_0^\infty \phi(k)\eta(k)G(k,E)\,\mathrm{d}k \tag{1}$$

where $\eta(k)$ is the detector efficiency and $G(k,E)$ is the detector's response function. For a monochromatic photon beam with energy k, $G(k,E)$ can be considered as a scaled energy spectrum,

$$M(E) = c_k G(k,E), \tag{2}$$

where c_k is a scaling factor. Therefore, the response function can be modeled based on the energy spectra of radioactive sources that emit photons at discrete energy levels.

$G(k, E)$ is modeled using four sub-functions,

$$G(k, E) = G_1(k, E) + G_2(k, E) + G_3(k, E) + G_4(k, E) \tag{3}$$

$$G_1(k, E) = a_1 \exp\left(-\frac{(E-k)^2}{3.63^2}\right) \tag{4}$$

$$G_2(k, E) = 0.29 a_1 \exp\left(\frac{E-k}{8.00}\right) \operatorname{erfc}\left(\frac{E-k}{3.63\sqrt{2}}\right) \tag{5}$$

$$G_3(k, E) = \frac{a_3(k)}{2} \exp\left(-\frac{E}{95.24}\right) \operatorname{erfc}\left(\frac{E-k}{3.63\sqrt{2}}\right) \tag{6}$$

$$G_4(k, E) = 0.06 a_1 \left(\exp\left(-\frac{(E-E_{Cd,K_\alpha})^2}{3.63^2}\right) + \exp\left(-\frac{(E-E_{Te,K_\alpha})^2}{3.63^2}\right)\right) \tag{7}$$

where erfc is the complementary error function, defined as $\operatorname{erfc}(x) = 1 - \operatorname{erf}(x)$.

$G_1(k, E)$ is a Gaussian photopeak, where the statistical broadening of the gamma-ray photopeak is approximated by a Gaussian function. $G_2(k, E)$ describes a broadening of the photopeak below k due to the hole tailing on the low energy side, which contributes to the asymmetry of the photopeak. $G_3(k, E)$ is an inclined shelf structure below the photopeak, whose slope is represented by an exponential function. In both $G_2(k, E)$ and $G_3(k, E)$, the error function is used to impose that the photon counts are only effective below the photopeak energy at k. $G_4(k, E)$ describes the CdTe escape peaks, which comprises two Gaussian functions at the CdTe escape peak energies E_{Cd,K_α} and E_{Te,K_α}: $E_{Cd,K_\alpha} = k - 23.2$ keV and $E_{Te,K_\alpha} = k - 26.1$ keV. Each function is modeled using empirically determined parameters.

In Eq.(6), $a_3(k)$ detemines the height of the inclined shelf structure. In the measured spectra, it is observed that this parameter depends on k, as plotted in Figure 3. This parameter is modeled by fitting the measured value as

$$a_3(k) = \begin{cases} 0.43 a_1 & \text{if } k < 56.14 \\ a_1\left(2.01 e^{k/196.93} - 2.25\right) & \text{if } 56.14 \le k < 315.20 \\ a_1\left(1.30 \cdot 10^{-8} e^{k/17.39} + 6.74\right) & \text{if } k \ge 315.20 \end{cases} \tag{8}$$

The height of the Gaussian peak $G_1(k, E)$, a_1, can be calculated by im-

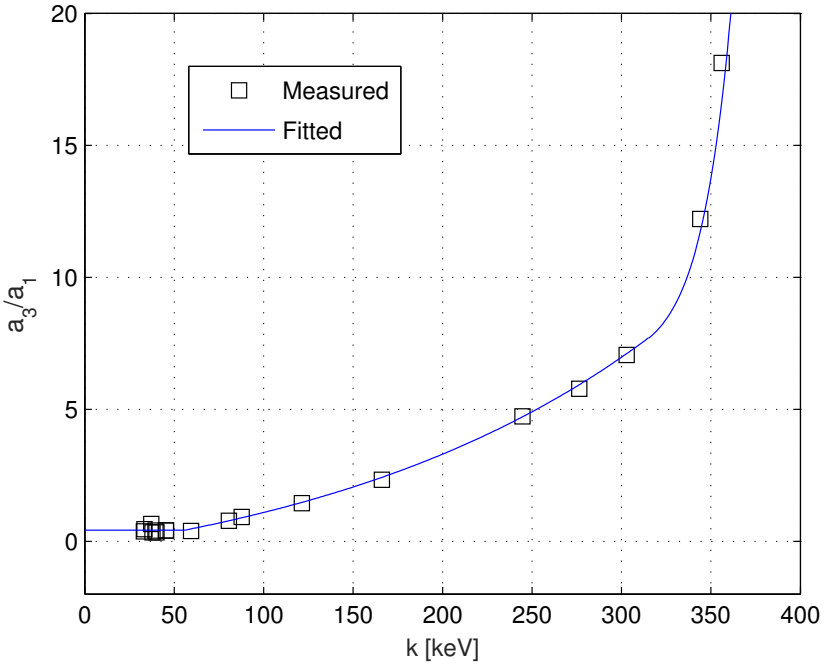

Figure 3: (Squares) the ratio of a_3 to a_1 determined by fitting the measured spectra. (Line) the fitted line described in Eq.(8).

posing the normalization condition

$$\int_0^\infty G(k, E)\,\mathrm{d}E = 1. \tag{9}$$

An example of the modeled response function for $k = 80$ keV is plotted in Figure 4.

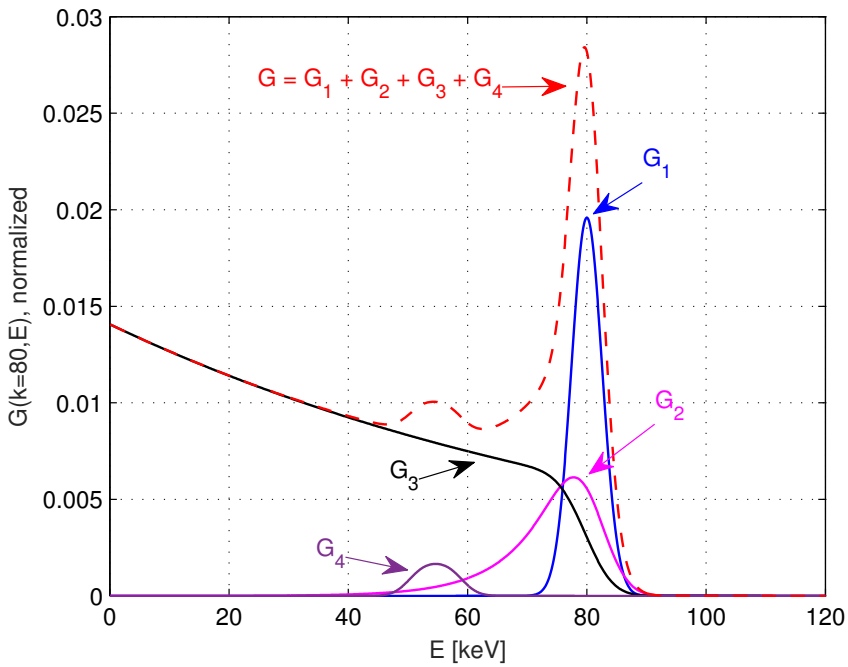

Figure 4: Response function model for $k = 80$ keV, $G(k = 80, E)$.

4. Reconstruction of measured spectra

In order to demonstrate that the response function modeled in the last section correctly describes the response of the detector, the energy spectra measured in Section 2 are reconstructed. For a radioactive source emitting photons with discrete energy levels, the measured energy spectrum can be reconstructed by adding Eq.(2) over all relevant energy photon beams,

$$M(E) = \sum_{i=1}^{N} c_i G(k_i, E) \tag{10}$$

where $M(E)$ is the reconstructed spectrum, c_i is a scaling factor for the photon beam with energy k_i and N is the number of discrete energy levels.

Figure 5 presents the reconstruction of the measured spectra using the response function from the R5-X2 synthetic diagnostic module (old, simplified model) [2] and the one modeled in the previous section (new model). Only energy spectra with a single gamma-ray photopeak at k_γ are considered, and the contribution from the fluorescent X-rays below 40 keV is not taken into account. Thus the reconstruction is done by multiplying a single scaling constant by the response function, $M(E) = c_\gamma G(k_\gamma, E)$. Whereas the new model fits well the measured spectra of ^{241}Am, ^{109}Cd, and ^{139}Ce, the old model cannot reproduce the continuous spectrum below the photopeak since it includes only the photopeak and the spectrum below the Compton edge, which is distant from the photopeak.

The energy spectra and the reconstruction of the radioactive sources which have several gamma-ray photopeaks, ^{152}Eu and the multi-isotope source, are plotted in Figure 6. The spectra of these sources can be reconstructed as

$$\begin{aligned} M_{tot}(E) &= \sum_{i=1}^{N_\gamma} M_{\gamma i} + M_0 + M_{Pb} \\ &= \sum_{i=1}^{N_\gamma} c_{\gamma i} G(k_{\gamma i}, E) + M_0 + c_{Pb} G(k_{Pb}, E) \end{aligned} \tag{11}$$

where $M_{tot}(E)$ is a reconstructed spectrum and M_0 is a flat offset count given by gamma-rays with energies above the measurement limit, about 440 keV. M_{Pb} describes the fluorescent X-rays emitted from the lead shielding at k_{Pb}=75.0. ^{152}Eu has three significant gamma-ray lines within the mea-

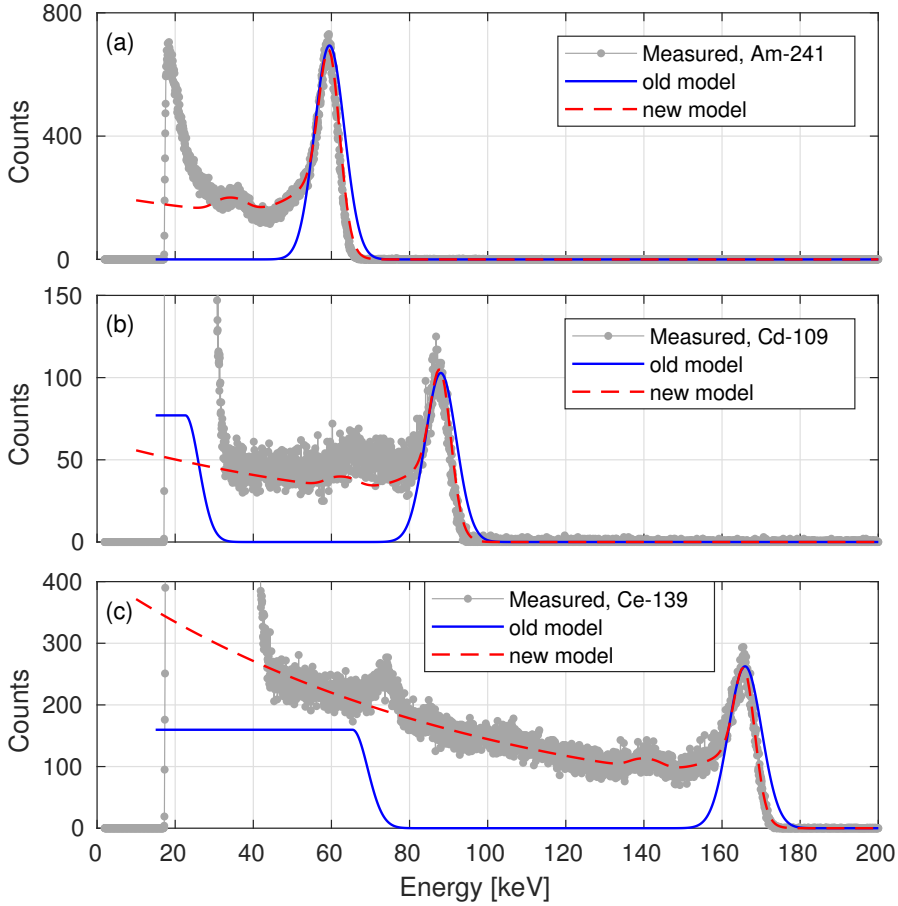

Figure 5: Measured energy spectrum (dot-line) and reconstruction using the default response function from R5-X2 (old model) and the one modeled in this work (new model), for (a) ^{241}Am (k_γ=59.9, c_γ=1.53·10^4), (b) ^{109}Cd (k_γ=88.0, c_γ=4.43·10^3), (c) ^{139}Ce (k_γ=159.9, c_γ=3.45·10^4). Fluorescent X-rays from the lead shielding appear near 75 keV.

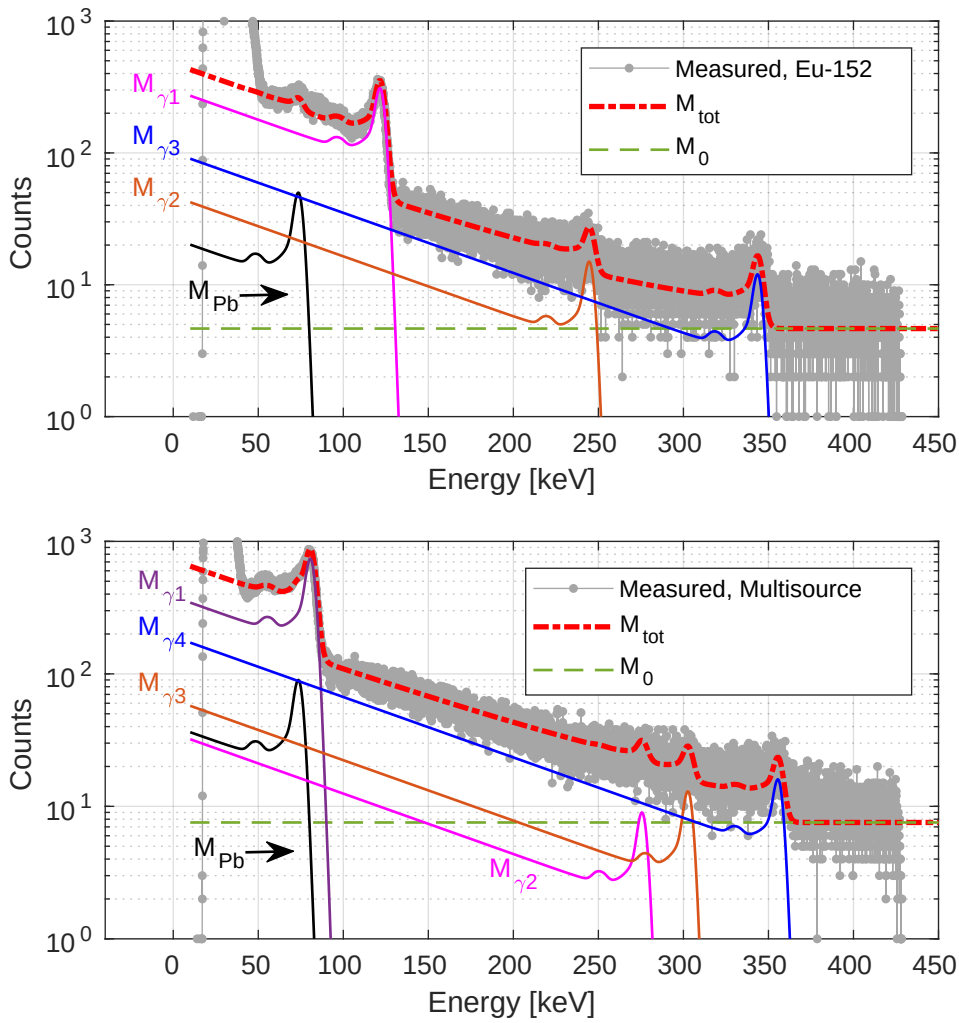

Figure 6: Reconstruction of the energy spectrum of (a) ^{152}Eu and (b) multi-isotope source.

surement limit, thus N_γ is 3. The multi-isotope source has four significant gamma-ray lines within the measurement limit, all from ^{133}Ba, thus N_γ is 4. The detailed parameters are summarized in Tables 2 and 3.

M_0	4.65	c_{Pb}	$1.37{\cdot}10^3$
$k_{\gamma 1}$	122.8	$c_{\gamma 1}$	$2.05{\cdot}10^4$
$k_{\gamma 2}$	244.7	$c_{\gamma 2}$	$3.82{\cdot}10^3$
$k_{\gamma 3}$	344.3	$c_{\gamma 3}$	$8.47{\cdot}10^3$

Table 2: Parameters used in Eq.(11) to reconstruct the energy spectrum of ^{152}Eu in Figure 6.

M_0	7.56	c_{Pb}	$2.46{\cdot}10^3$
$k_{\gamma 1}$	81.0	$c_{\gamma 1}$	$2.36{\cdot}10^4$
$k_{\gamma 2}$	276.4	$c_{\gamma 2}$	$2.95{\cdot}10^3$
$k_{\gamma 3}$	302.9	$c_{\gamma 3}$	$5.34{\cdot}10^3$
$k_{\gamma 4}$	356.0	$c_{\gamma 4}$	$1.61{\cdot}10^4$

Table 3: Parameters used in Eq.(11) to reconstruct the energy spectrum of Multi-isotope in Figure 6.

In Figure 7, the full spectrum of ^{139}Ce is reconstructed as M_{tot}, including the fluorescent X-rays from ^{139}Ce and the lead shielding,

$$\begin{aligned} M_{tot}(E) =& M_\gamma + M_{K\alpha 1} + M_{K\alpha 2} + M_{K\beta 1} + M_{K\beta 2} + M_{Pb} \\ =& c_\gamma G(k_\gamma, E) + c_{K\alpha 1} G(k_{K\alpha 1}, E) + c_{K\alpha 2} G(k_{K\alpha 2}, E) \\ &+ c_{K\beta 1} G(k_{K\beta 1}, E) + c_{K\beta 2} G(k_{K\beta 2}, E) + c_{Pb} G(k_{Pb}, E), \end{aligned} \tag{12}$$

where the parameters used in the reconstruction are summarized in Table 4. Since the K line emissions of ^{139}Ce are closely spaced and interfere each other, the coefficients of $M_{K\alpha 2}$, $M_{K\beta 1}$, and $M_{K\beta 2}$ are determined using the relative probabilities of these lines to $K\alpha 1$ line from the reference [18].

k_{Pb}	75.0	c_{Pb}	960.34
k_{γ}	165.9	c_{γ}	$2.88 \cdot 10^4$
$k_{K\alpha 1}$	33.4	$c_{K\alpha 1}$	$1.16 \cdot 10^4$
$k_{K\alpha 2}$	33.0	$c_{K\alpha 2}/c_{K\alpha 1}$	0.55
$k_{K\beta 1}$	37.2	$c_{K\beta 1}/c_{K\alpha 1}$	0.18
$k_{K\beta 2}$	37.8	$c_{K\beta 2}/c_{K\alpha 1}$	0.09

Table 4: Parameters used in Eq.(12) to reconstruct the energy spectrum of ^{139}Ce in Figure 7.

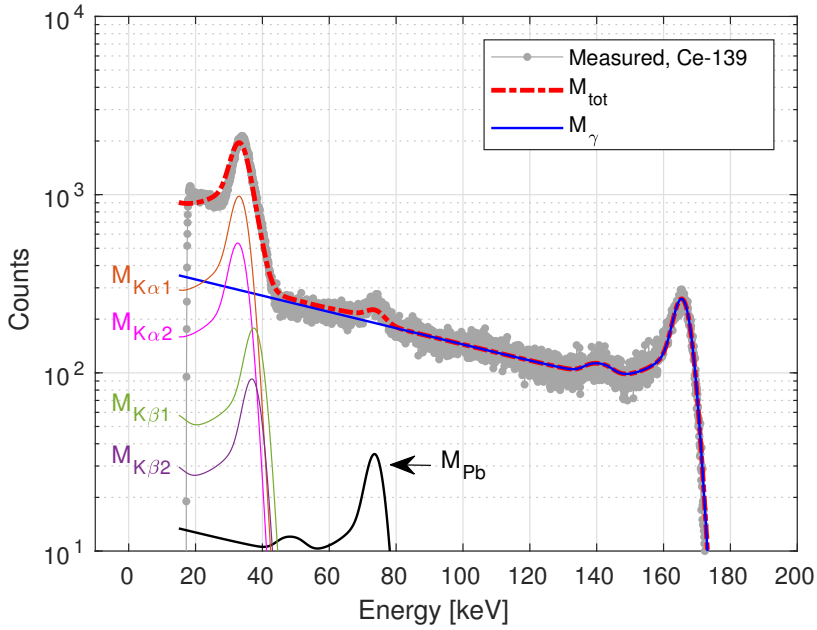

Figure 7: Reconstruction of the energy spectrum of ^{139}Ce.

5. Application of the synthetic diagnostic

The response function modeled in this work has been implemented in the hard X-ray synthetic diagnostic R5-X2 [2], which is coupled to the Fokker-Planck code LUKE [12]. The structure of the calculation procedure is presented in Figure 8: after each tokamak experiment, the electron distribution function $f_e(t, \boldsymbol{X}, \boldsymbol{p})$, in the real($\boldsymbol{X}$) and momentum($\boldsymbol{p}$) spaces can be modeled by solving the Fokker-Planck equation. As input parameters, the plasma equilibrium is reconstructed by the equilibrium code LIUQE [19], plasma

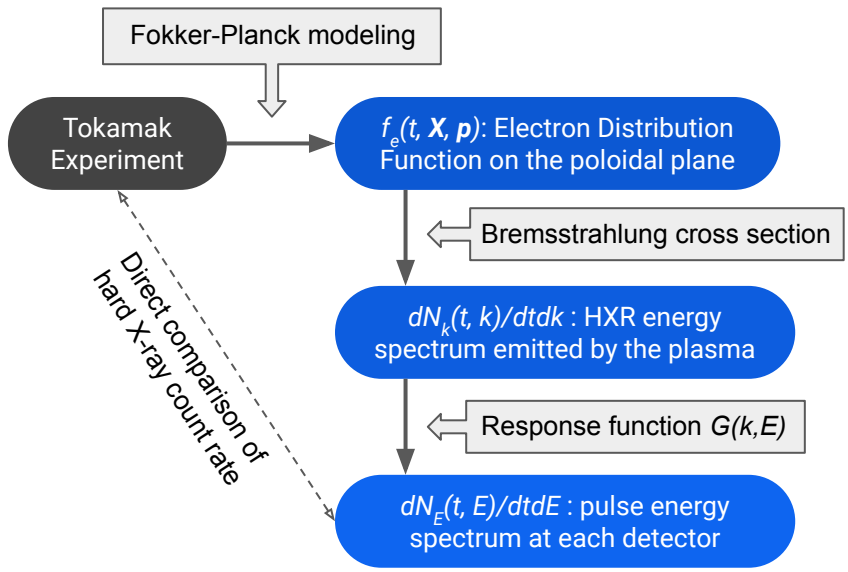

Figure 8: Workflow of the hard X-ray synthetic diagnostic coupled to the Fokker-Planck modeling of tokamak plasma.

density and temperature profiles are loaded from the Thomson scattering diagnostic data, and the loop voltage is loaded from the flux loop measurement. For the modeling of TCV ECCD plasmas, the code is coupled to the ray tracing code C3PO [20], so the damping of the EC rays can be calculated self-consistently.

The modeled electron distribution function $f_e(t, \boldsymbol{X}, \boldsymbol{p})$ can be directly loaded in the R5-X2 module, as well as the equilibrium structure. The distribution function is used to calculate the effective photon energy spectrum $dN_k(t,k)/(dtdk)$ using the bremsstrahlung cross section $d\sigma/(dtdkd\Omega)$, where $d\Omega$ is a solid angle and k is a photon energy. Then the photon spectrum arrived at each detector $dN_k(t,k)/(dtdk)$ is used to calculate the pulse energy spectrum $dN_E(t,E)/(dtdE)$ [2],

$$\frac{dN_E(t,E)}{dtdE} = \int_0^\infty \eta_A(k)\,(1-\eta_D(k))\,G(k,E)\frac{dN_k(t,k)}{dtdk}dk. \tag{13}$$

Here, $\eta_A(k)$ is the ratio of photons transmitted on their way to the detector;

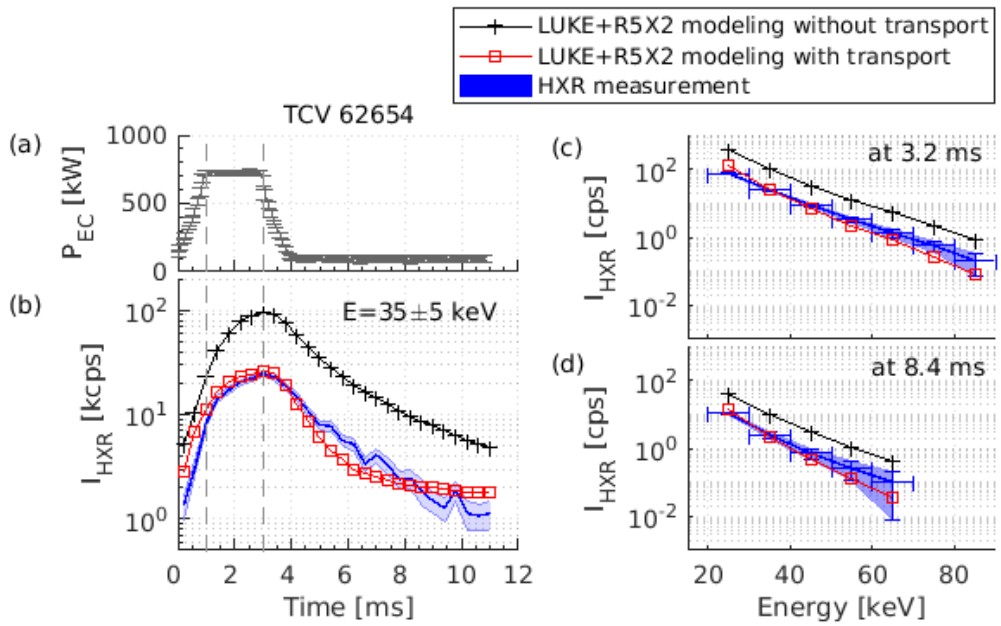

Figure 9: Example of an application of the hard X-ray synthetic diagnostic (R5-X2) coupled with the Fokker-Planck modeling (LUKE). (a) Modulated ECCD power during a TCV operation. (b) Time evolution of hard X-ray count rate in the energy bin of $E = 35 \pm 5$ keV. (c,d) Energy spectrum of hard X-ray count rate at 3.2 ms and 8.4 ms.

this can decrease due to the absorption by the window or absorber structures placed in front of the detector. $(1 - \eta_D(k))$ describes the fraction of photons stopped inside the detector volume, therefore having a photon-matter interaction. $G(k, E)$ is the normalized detector's response function, $\int_0^\infty G(k, E)dk = 1$.

Figure 9 shows an example of the hard X-ray synthetic diagnostic application in the TCV tokamak, where the simulation and measurement results are compared [21]. In the experiment analyzed in Figure 9, 750 kW of EC wave pulses were injected to study the response of suprathermal electrons to ECCD. The hard X-ray photon counts measured by the detector were sorted into time bins of 0.4 ms and energy bins of 10 keV, then the data have been conditionally averaged over the repetitive EC wave pulses. Figure 9 (a) shows the shape of the injected EC wave during a pulse cycle. Blue lines in Figure 9 (b-d) represent the conditionally averaged hard X-ray count rate from channel 14 of the equatorial camera, whose line of sight is passing the

magnetic axis where the ECCD was localized.

In order to investigate the dynamics of suprathermal electrons, various anomalous transport models have been tested in the Fokker-Planck simulation. As an example, black cross and red square markers in Figure 9 (b-d) show the simulation results with different transport conditions. The simulation results from the synthetic diagnostic have shown that the hard X-ray count rate is overestimated without considering the anomalous transport, and an appropriate transport modeling is required to describe the multi-dimensional hard X-ray data. Various transport models which depend on time and real and momentum spaces have been used to investigate the origin of suprathermal electron transport, which can be attributed to turbulent or wave-induced transport [21].

6. Summary

A realistic response function is modeled for the CdTe detectors used in the HXRS apparatus of the TCV tokamak. The energy spectra of five radioactive sources, ^{241}Am, ^{109}Cd, ^{139}Ce, and ^{152}Eu, and a multi-isotope source, a liquid mixture of ^{133}Ba, ^{60}Co, and ^{137}Cs, are measured and analyzed. The characteristics of the detector observed in the measurement are considered in the response function modeling. The response function consists of four sub-functions: a Gaussian photopeak, an exponential decay at the energies below the photopeak, an inclined shelf structure which is exponentially increasing towards the low energy side, and the escape peaks by the CdTe material. The coefficients of the function are empirically determined based on the measured spectra.

In order to demonstrate the ability of the response function to correctly reproduce the response of the detector to photons, the response function is used to reconstruct the measured energy spectra. The reconstructed spectra using the new function fit well the measured spectra, while the default response function model in the synthetic diagnostic module cannot reproduce the continuous shelf structure below the photopeak. Also, the energy spectra which consist of several gamma-rays or fluorescent X-rays are also correctly reconstructed.

This new model has now been implemented in the synthetic diagnostic module and assists the analysis of the hard X-ray measurements in the TCV tokamak for the study of high-energy electron physics.

7. Acknowlegments

This work was supported in part by the Swiss National Science Foundation. This work has been carried out within the framework of the EUROfusion Consortium and has received funding from the Euratom research and training programme 2014 - 2018 and 2019 - 2020 under grant agreement No 633053. The views and opinions expressed herein do not necessarily reflect those of the European Commission.

References

[1] S. Coda, Review of Scientific Instruments 79 (2008) 10F501.

[2] Y. Peysson, J. Decker, Physics of Plasmas 15 (2008) 092509.

[3] R. W. Harvey, et al., Physical Review Letters 88 (2002) 205001.

[4] P. Nikkola, et al., Nuclear Fusion 43 (2003) 1343.

[5] C. Petty, et al., Nuclear Fusion 42 (2002) 1366.

[6] N. Bertelli, E. Westerhof, Nuclear Fusion 49 (2009) 095018.

[7] E. Poli, et al., Nuclear Fusion 53 (2012) 013011.

[8] S. Coda, et al., Nuclear Fusion 59 (2019) 112023.

[9] S. Gnesin, Electron Cyclotron Heating and Suprathermal Electron Dynamics in the TCV Tokamak, Ph.D. thesis, EPFL, Switzerland (2011).

[10] S. Coda, et al., in: 1st EPS conference on Plasma Diagnostics, Vol. 240, SISSA Medialab, 2016, p. 139.

[11] J. Kamleitner, et al., Nuclear Instruments and Methods in Physics Research Section A: Accelerators, Spectrometers, Detectors and Associated Equipment 736 (2014) 88.

[12] J. Decker, Y. Peysson, DKE: a fast numerical solver for the 3-D relativistic bounce-averaged electron Drift Kinetic Equation Tech. rep. No EUR-CEA-FC-1736 (2004).

[13] Y. Peysson, F. Imbeaux, Review of Scientific Instruments 70 (1999) 3987.

[14] G. W. Phillips, K. W. Marlow, Nuclear Instruments and Methods 137 (1976) 525–536.

[15] J. Campbell, et al., Nuclear Instruments and Methods in Physics Research Section B: Beam Interactions with Materials and Atoms 9 (1985) 71.

[16] R. Redus, et al., IEEE Transactions on Nuclear Science 56 (2009) 2524.

[17] J. E. Fernández, et al., X-Ray Spectrometry 44 (2015) 177.

[18] Chu, S.Y.F., Ekström, L.P. and Firestone, R.B., The Lund/LBNL Nuclear Data Search, Version 2.0, available at `http://nucleardata.nuclear.lu.se/toi/` (accessed on September 25th, 2018).

[19] F. Hofmann, G. Tonetti, Nuclear Fusion 28 (1988) 1871.

[20] Y. Peysson, et al., Plasma Physics and Controlled Fusion 54 (2012) 045003.

[21] D. Choi, Experimental analysis of suprathermal electrons generated by electron cyclotron waves in tokamak plasmas, Ph.D. thesis, EPFL, Switzerland (2020).